Autophagy protein microtubule-associated protein 1 light chain-3B (LC3B) activates extrinsic apoptosis during cigarette smoke-induced emphysema

Zhi-Hua Chen[a,b,1], Hilaire C. Lam[a,c,1], Yang Jin[a], Hong-Pyo Kim[a,d], Jiaofei Cao[a,b], Seon-Jin Lee[a], Emeka Ifedigbo[a], Harikrishnan Parameswaran[e], Stefan W. Ryter[a], and Augustine M. K. Choi[a,f,2]

[a]Division of Pulmonary and Critical Care Medicine, Brigham and Women's Hospital, Harvard Medical School, Boston, MA 02115; [b]Division of Respiratory Medicine, Second Hospital of Zhejiang University School of Medicine, Hangzhou 310009, People's Republic of China; [c]Cellular and Molecular Pathology Program, University of Pittsburgh School of Medicine, Pittsburgh, PA 15261; [d]School of Biological Sciences, College of Natural Sciences, University of Ulsan, Ulsan 680-749, Korea; [e]Department of Biomedical Engineering, Boston University, Boston, MA 02118; and [f]College of Medicine, Kyung Hee University, Seoul 130-701, Korea

Edited by John D. Minna, University of Texas Southwestern Medical Center, Dallas, TX, and accepted by the Editorial Board September 22, 2010 (received for review April 23, 2010)

Chronic obstructive pulmonary disease (COPD) is a debilitating disease caused by chronic exposure to cigarette smoke (CS), which involves airway obstruction and alveolar loss (i.e., emphysema). The mechanisms of COPD pathogenesis remain unclear. Our previous studies demonstrated elevated autophagy in human COPD lung, and as a cellular and tissue response to CS exposure in an experimental model of emphysema in vivo. We identified the autophagic protein microtubule-associated protein 1 light chain-3B (LC3B) as a positive regulator of CS-induced lung epithelial cell death. We now extend these initial observations to explore the mechanism by which LC3B mediates CS-induced apoptosis and emphysema development in vivo. Here, we observed that *LC3B*$^{-/-}$ mice had significantly decreased levels of apoptosis in the lungs after CS exposure, and displayed resistance to CS-induced airspace enlargement, relative to WT littermate mice. We found that LC3B associated with the extrinsic apoptotic factor Fas in lipid rafts in an interaction mediated by caveolin-1 (Cav-1). The siRNA-dependent knockdown of Cav-1 sensitized epithelial cells to CS-induced apoptosis, as evidenced by enhanced death-inducing signaling complex formation and caspase activation. Furthermore, *Cav-1*$^{-/-}$ mice exhibited higher levels of autophagy and apoptosis in the lung in response to chronic CS exposure in vivo. In conclusion, we demonstrate a pivotal role for the autophagic protein LC3B in CS-induced apoptosis and emphysema, suggestive of novel therapeutic targets for COPD treatment. This study also introduces a mechanism by which LC3B, through interactions with Cav-1 and Fas, can regulate apoptosis.

Chronic obstructive pulmonary disease (COPD), ranked among the world's foremost health problems, is characterized by airway inflammation and destructive emphysema (1, 2). Exposure to cigarette smoke (CS) is a major risk factor for COPD development, which occurs in approximately 15% of smokers. The pathogenesis of COPD remains incompletely elucidated, and may involve imbalance of cellular protease/antiprotease activities as well as oxidative stress (3). Recent studies also implicate lung cell apoptosis as a possible mechanism for COPD development (4, 5). The role of nonapoptotic programmed cell death or survival mechanisms (i.e., autophagy) remain unclear at present.

Recently, we have demonstrated the increased occurrence of cellular macroautophagy (hereafter, autophagy) in human lung tissue from patients with COPD, and as a general response to CS exposure in rodent lungs or epithelial cells (6, 7). Autophagy refers to a homeostatic process for the turnover of cellular organelles and protein (8–10). During autophagy, double-membraned autophagic vacuoles (AVs) or autophagosomes surround cytosolic organelles (e.g., endoplasmic reticulum, mitochondria) or protein, and subsequently fuse with lysosomes, where the engulfed components are degraded by lysosomal hydrolases. By regenerating metabolites (i.e., amino acids, fatty acids) for anabolic pathways, autophagy can prolong survival during starvation. Currently, more than 30 autophagy-related genes and gene products critical in the regulation of autophagy, designated "*atg*," have been identified in yeast and higher mammals (10). Among these, the microtubule-associated protein 1 light chain 3 (LC3; *yeast*, Atg8) is cleaved from a proform by Atg4 and then conjugated with phosphatidylethanolamine by the sequential action of Atg7 and Atg3 (10). In mammals, the conversion of LC3 from LC3-I (free form) to LC3-II (phosphatidylethanolamine-conjugated form) represents a key step in autophagosome formation (11).

Autophagy provides essential functions in the maintenance of cellular homeostasis and adaptation to adverse environments (8–10). The induction of autophagy to greater than basal levels occurs in response to diverse stimuli including nutrient starvation, cytokines, and oxidative stress. However, excessive autophagy may be associated with the activation of programmed cell death (i.e., apoptosis) through a cell-autodigestive process (12, 13). The role of autophagy, whether protective or deleterious, in human diseases, or specifically in chronic lung disease remains obscure. As apoptosis is implicated in COPD pathogenesis (4, 5), we have investigated the potential relationships between autophagy and apoptosis in a mouse model of CS-induced emphysema. In particular, we have examined the regulatory role of the autophagic protein LC3B in apoptosis pathways induced by CS.

Results

To investigate the role of the autophagic protein LC3B in emphysema development, *LC3B*$^{-/-}$ mice, WT littermate (*LC3B*$^{+/+}$), or C57BL/6 mice were subjected to CS exposure for 3 mo, and their lungs were analyzed for airspace enlargement, apoptosis, and autophagy. Consistent with previous observations (14, 15), C57BL/6 WT mice displayed marked increases in lung airspace after 12-wk CS exposure relative to air-treated controls, as determined by comparative histologic examination (Fig. S1) and mean linear intercept (MLI) measurements (Fig. 1*A*). Similarly, *LC3B*$^{+/+}$ WT littermate mice exposed to CS for 12 wk displayed marked increases in lung airspace after CS exposure relative

Author contributions: Z.-H.C. designed research; Z.-H.C., H.C.L., Y.J., J.C., S.-J.L., and E.I. performed research; H.C.L. and H.P. contributed new reagents/analytic tools; Z.-H.C., H.-P.K., H.P., S.W.R., and A.M.K.C. analyzed data; and S.W.R. wrote the paper.

The authors declare no conflict of interest.

This article is a PNAS Direct Submission. J.D.M. is a guest editor invited by the Editorial Board.

[1]Z.-H.C. and H.C.L. contributed equally to this work.

[2]To whom correspondence should be addressed. E-mail: amchoi@rics.bwh.harvard.edu.

This article contains supporting information online at www.pnas.org/lookup/suppl/doi:10.1073/pnas.1005574107/-/DCSupplemental.

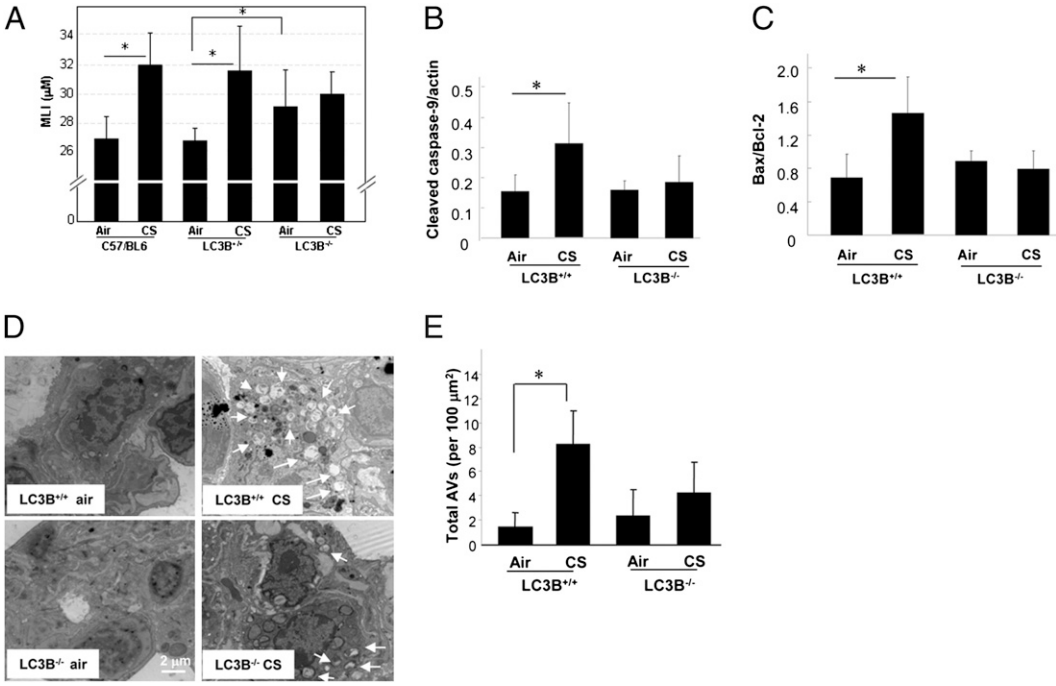

Fig. 1. LC3B regulates CS-induced autophagy, apoptosis, and emphysematous airspace enlargement in vivo. WT C57BL/6, $LC3B^{+/+}$, or $LC3B^{-/-}$ mice were exposed to chronic CS exposure or air for 3 mo (C57BL/6, $n = 9$ for air, $n = 8$ for CS; $LC3B^{+/+}$, $n = 6$ for air, $n = 9$ for CS; $LC3B^{-/-}$, $n = 9$ for air, $n = 9$ for CS). (*A*) Quantification of MLIs (*$P < 0.01$). Representative images of mouse lungs with H&E staining are shown in Fig. S1. Western blot analysis and corresponding quantification for cleaved caspase-9 (*B*) and Bax/Bcl-2 ratio (*C*) in CS-exposed mouse lungs. Data are means ± SD; N.S., not significant; *$P < 0.05$. (*D*) Representative EM of mouse lung sections. Arrows indicate autophagic vacuoles (AVs). (*E*) EM images scored for number of AVs. The data are represented as AVs per 100 μm^2; $n = 20$ images representative of each group; *$P < 0.05$.

to air-treated controls. In contrast, airspace was not increased in $LC3B^{-/-}$ mouse lungs by CS exposure relative to air-treated controls. $LC3B^{-/-}$ mice exhibited significant basal airspace enlargement relative to WT littermate mice by MLI (Fig. 1*A*).

Airspace enlargement caused by CS exposure in $LC3B^{-/-}$ and WT mice was also assessed separately by measuring the equivalent diameter of alveolar airspaces using a previously published automated image processing algorithm (16). Consistent with the MLI measurements, the equivalent diameter of CS-exposed $LC3B^{+/+}$ mice (31.5 ± 1.6 μm) was significantly greater than air-treated $LC3B^{+/+}$ mice (27.9 ± 1.4 μm; $P = 0.001$), whereas the equivalent diameter of CS-exposed $LC3B^{-/-}$ mice (30.7 ± 1.8 μm) was not different from the air-treated $LC3B^{-/-}$ mice (29.0 ± 3.1 μm). The equivalent diameter of air-treated $LC3B^{-/-}$ mice was greater than that of the air-treated $LC3B^{+/+}$ mice; however, the increase was not statistically significant.

Staining of lung vasculature with α-smooth muscle actin revealed vascular remodeling in CS-exposed WT mice that was not evident in CS exposed $LC3B^{-/-}$ mice (Fig. S2).

To investigate lung cell death, we measured apoptotic indices (i.e., cleaved caspase-9, Bax/Bcl-2 ratio). These markers were significantly increased in the lungs of $LC3B^{+/+}$ mice by CS exposure, but were not increased in CS-exposed $LC3B^{-/-}$ mice (Fig. 1 *B* and *C*). Furthermore, CS induced the accumulation of autophagic vacuoles or AVs as determined by EM, a gold standard morphological readout for evidence of autophagy, in the lungs of WT ($LC3B^{+/+}$) mice. In contrast, a reduced number of AVs were detected in the lung after CS exposure in the $LC3B^{-/-}$ mice (Fig. 1 *D* and *E*).

To explore the mechanisms by which LC3B regulates CS-induced epithelial cell apoptosis, we examined whether LC3B can interact with known apoptosis-related factors. In mammalian cells, the "extrinsic" apoptotic pathway responds to stimuli via activation of death receptor family proteins (i.e., Fas) (17, 18). Stimulation with aqueous CS extract (CSE) induced the extrinsic apoptotic pathway in lung epithelial (Beas-2B) cells, involving death-inducing signaling complex (DISC) formation, caspase-8 activation, and Bax activation (Fig. S3 *A*–*C*). We examined whether LC3B can interact with mediators of this pathway. LC3B interacted with Fas under basal conditions in Beas-2B cells, whereas this interaction was rapidly disrupted after exposure to CSE (Fig. 2 *A* and *B*). Confocal imaging revealed that LC3B and Fas colocalized in the plasma membrane under basal conditions (Fig. 2*B*), whereas the merged complex of LC3B and Fas at the cell membrane disappeared after CSE treatment.

Fas-mediated apoptosis involves the association of Fas with accessory molecules (i.e., procaspase-8, FADD). Recent studies show that Fas can localize to plasma membrane lipid rafts (19, 20). We therefore examined whether LC3B localizes to lipid rafts. Subcellular fractionation experiments demonstrated that LC3B and Fas also localized to low-density caveolin-1 (Cav-1) containing fractions under basal conditions in Beas-2B cells and lung fibroblasts (Fig. 2*C*). Cav-1 serves as structural component of caveolae, which are cholesterol- and glycosphingolipid-rich domains of the plasma membrane. As Cav-1 interacts with several membrane-associated signaling proteins (21), we examined whether Cav-1 can mediate the LC3B-Fas interaction. Cav-1, under basal conditions, interacted with both LC3B and Fas by coimmunoprecipitation assays (Fig. 2*D*) and confocal imaging studies (Fig. S4). Interestingly, both Cav-1-Fas and LC3B-Cav-1 complexes dissociated after CSE treatment (Fig. 2*D*). Treatment of Beas-2B cells with siRNA targeting LC3B increased the basal interaction of Cav-1 with Fas (Fig. 3*A*). Furthermore, Beas-2B cells infected with LC3B-siRNA exhibited reduced DISC formation and Bax activation in response to CSE relative to control-infected cells (Fig. 3*A*).

Proteins that bind Cav-1 typically contain canonical Cav-1-binding motifs (CBMs), ΦXΦXXXXΦ or ΦXXXXΦXXΦ,

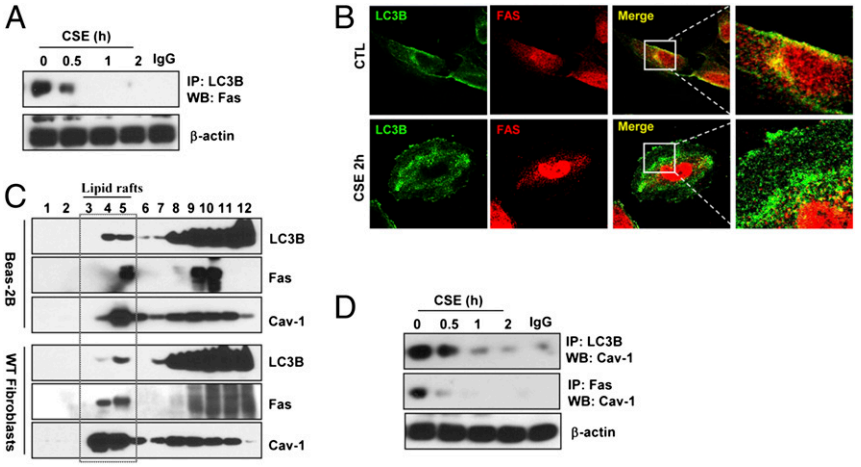

Fig. 2. LC3B-Cav-1-Fas interactions regulate CSE-induced autophagic and apoptotic cell death. (*A*) CSE-disrupted the LC3B-Fas interaction. Beas-2B cells were treated with CSE (10%) for the indicated times and their lysates were immunoprecipitated (IP) with anti-LC3B and Western immunoblotted (WB) for Fas. Cellular β-actin served as the standard. (*B*) Representative immunofluorescence images of LC3B and Fas staining in Beas-2B cells. Colocalization is indicated by the merged images (*Right*). (*C*) LC3B and Fas partially localize in lipid rafts. Beas-2B cells or WT fibroblasts were fractionated by sucrose-gradient ultracentrifugation and the fractions were immunoblotted for Fas, LC3B, and Cav-1. (*D*) CSE-disrupted the LC3B-Cav-1 and Fas-Cav-1 interaction. Cells were exposed to CSE (10%) for the indicated times, and their lysates were subjected to IP with anti-LC3B or Fas, and analyzed by WB for Cav-1. β-Actin served as the standard.

where Φ is an aromatic amino acid (W, F, or Y) and X is any nonaromatic amino acid, although proteins without such motifs are also capable of binding to Cav-1 (22). The primary structure of LC3B contains a sequence ^{108}FLYMVYASQETF^{119} (LC3B Cav-1 binding motif), resembling a consensus CBM. To examine whether this sequence mediates the LC3B-Cav-1 interaction, we generated amino acid substitution mutants of LC3B at position Y113. Interestingly, the Y113A mutation, an aromatic-to-non-aromatic amino acid substitution, abolished the basal LC3B-Cav-1 interaction (Fig. 3*B*). Similar to observations made with LC3B-siRNA, transfection with LC3B Y113A increased the Cav-1-Fas interaction (Fig. 3*B*). Overexpression of WT LC3B in Beas-2B cells markedly augmented cell death in response to CSE treatment. By comparison, overexpression of LC3B Y113A (Fig. 3*C*)

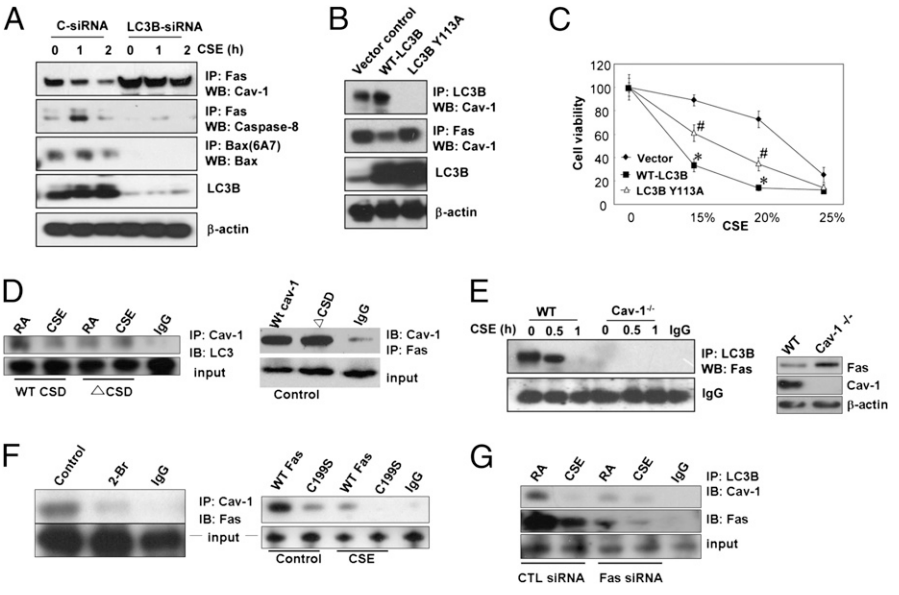

Fig. 3. LC3B regulates Fas-mediated apoptosis in CSE-treated Beas-2B cells through binding interactions with Cav-1 and Fas. (*A*) Beas-2B cells were pretreated with control siRNA (C-siRNA) or LC3B-siRNA for 48 h, followed by CSE (10%) treatment for the indicated times. The lysates were then subjected to IP and WB analysis as indicated. (*B*) Mutation of LC3B at Y113 modulates the LC3B-Cav-1-Fas interactions under basal conditions. Beas-2B cells were transfected with WT or Y113A LC3B for 48 h, and the cell lysates were then subjected for IP and WB analysis as indicated. (*C*) Beas-2B cells were transfected with WT LC3B or mutant Y113A LC3B for 48 h, followed by the CSE treatment for an additional 24 h. Cells were then subjected to the 3-(4,5-dimethylthiazol-2-yl)-2,5-diphenyl tetrazolium bromide cell viability assay. Data represent mean ± SD; $^{*}P < 0.05$ vs. corresponding vector control values; $^{\#}P < 0.05$ vs. corresponding values for WT-LC3B overexpression. (*D*) WT cav-1 and ΔCSD expression clones were transfected into Beas2B cells; 36 h after transfection, cells were exposed to CSE (10%). After 1 h, cell lysates were immunoprecipitated with anti-Cav-1 rabbit polyclonal antibodies. After separation on SDS/PAGE, respective mouse monoclonal antibodies were used to detect the interactions between Cav-1 and LC3B or Cav-1 and Fas, as indicated. The figure is representative of at least three independent experiments. (*E*) Cell lysates from 10% CSE-treated WT or *Cav-1*$^{-/-}$ fibroblasts were subjected to IP by LC3B and WB for Fas. A nonspecific IgG band served as the standard. The expression of Cav-1 and Fas in *Cav-1*$^{-/-}$ fibroblasts were assessed by Western analysis (*Right*), using β-actin as the standard. (*F*) Fas-Cav-1 interaction depends on palmitoylation domains. (*Left*) Beas2B cells were pretreated for 1 h with 100 μM 2-bromopalmitate (2-Br) or DMSO as a control. Cell lysates were subjected to coimmunoprecipitation assays. The figure is representative of at least three independent experiments. (*Right*) WT Fas and C199S mutant expression clones were transfected into Beas2B cells; 36 h after transfection, cells were exposed to CSE (10%). After 1 h, cell lysates were immunoprecipated with anti-Cav-1 or anti-Fas rabbit polyclonal antibodies. After fractionation on SDS/PAGE, respective mouse monoclonal antibodies were used as primary antibodies to detect interaction between Cav-1 and Fas. The figure is representative of at least three independent experiments. (*G*) Beas-2B cells were pretreated with control siRNA (C-siRNA) or Fas-siRNA for 48 h, followed by CSE (10%) treatment for the indicated times. The lysates were subjected to immunoprecipitation (IP) and Western blot (WB) analysis as indicated.

also induced cell death, although to a lesser degree than the WT LC3B construct. These experiments suggest that LC3B promotes CSE-induced cell death, in part through a mechanism dependent on the Cav-1-binding motif.

To further explore the mechanisms by which Cav-1 facilitates Fas and LC3B interaction, we determined the binding sites of LC3B on Cav-1. We found that the Cav-1 scaffolding domain (CSD) is crucial to anchor LC3B in this complex. We transfected Beas2B cells WT Cav-1 or with Cav-1 bearing a mutated CSD (ΔCSD) and then assessed the interaction between LC3B and Cav-1 by coimmunoprecipitation (Fig. 3*D*). Cells transfected with Cav-1 ΔCSD showed decreased interaction between LC3B and Cav-1 relative to cells transfected with the WT Cav-1 construct (Fig. 3*D*). In contrast, Fas binding was not affected by the ΔCSD mutation (Fig. 3*D*). These data indicate that LC3B interacts with Cav-1 through interaction between the LC3B CBM and the Cav-1 CSD domains. In lung fibroblasts derived from *Cav-1*$^{-/-}$ mice, the LC3B-Fas interaction was diminished, suggesting an intermediate role for Cav-1 in complex formation (Fig. 3*E*). Total Fas expression slightly increased in *Cav-1*$^{-/-}$ cells (Fig. 3*E*, *Right*).

We next examined the nature of the binding between Fas and Cav-1. As Fas binding to Cav-1 was not abolished by the ΔCSD mutation, we explored additional possible binding sites. Cav-1 has three sites of palmitoylation in proximity to the COOH terminal. In Beas2B cells pretreated with 2-bromopalmitate, a general palmitoylation inhibitor, the interaction between Cav-1 and Fas was diminished (Fig. 3*F*). We then transfected Beas2B cells with a Fas mutant in which cysteine 199, a known palmitoylation site, was mutated to serine (C199S). Transfection with Fas C199S abolished the interaction between Fas and Cav-1 (Fig. 3*F*). These results suggest that Fas and Cav-1 interact through palmitoylation domains. Finally, treatment of Beas-2B cells with siRNA targeting Fas diminished the Cav-1-LC3B interaction (Fig. 3*G*). Taken together, these results suggest the interdependence of all three factors in complex formation, with the binding of Fas and LC3B occurring at distinct sites on the Cav-1 molecule.

The role of Cav-1 in pulmonary diseases remains controversial, and can have protective (23–25) or deleterious (26, 27) functions. Furthermore, the role of Cav-1 in COPD pathogenesis remains poorly understood. Here, we examined the role of Cav-1 in the regulation of CS-induced autophagy and cell death. In Cav-1-siRNA infected Beas-2B cells, CSE induced accumulation of autophagic vacuoles was enhanced relative to control infected cells (Fig. 4*A*). Furthermore, Cav-1-siRNA-infected cells displayed enhanced accumulation of LC3B-II relative to control siRNA-infected cells (Fig. 4*B*). In Cav-1-siRNA-treated Beas-2B cells, CSE treatment induced higher levels of apoptosis, as evidenced by the increased cleavage of caspase-3 and poly(ADP ribose) polymerase (Fig. 4*C*). Cav-1-siRNA-treated Beas-2B cells (Fig. 4*D*) were more susceptible to CSE-induced cell death. To further delineate the role of Cav-1 in CS-induced cellular responses, *Cav-1*$^{-/-}$ or WT mice were exposed to CS inhalation for 12 wk. Consistent with the in vitro findings, CS-exposed *Cav-1*$^{-/-}$ mice exhibited significantly higher levels of autophagy, as evidenced by increased accumulation of AV (Fig. 5*A*) and LC3B-II (Fig. 5*B*). CS-exposed *Cav-1*$^{-/-}$ mice exhibited significantly higher levels of apoptosis, as evidenced by activation of caspase-9 in the lung (Fig. 5*C*). Although the *Cav-1*$^{-/-}$ mice also had a basal lung airspace enlargement, they were more susceptible to the CS-induced lung injury and displayed a further enlarged airspace (Fig. 5*D* and Fig. S5).

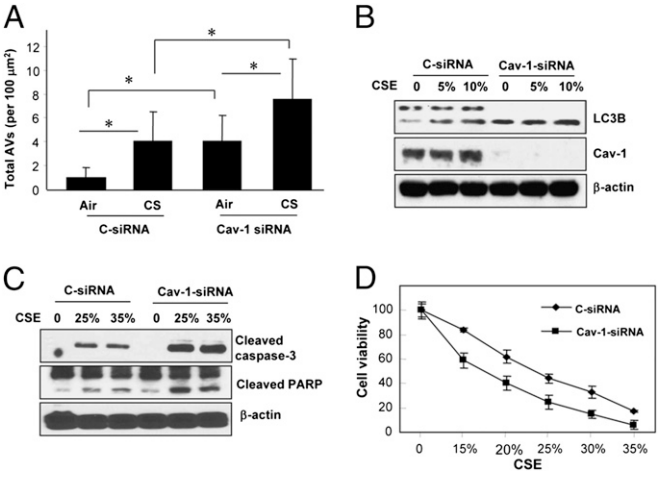

Fig. 4. Cav-1 suppresses CSE-induced autophagy and apoptotic cell death in Beas-2B cells. (*A*–*C*) Cells were transfected with siRNA for 48 h, followed by CSE treatment (10%) for an additional 24 h. (*A*) EM images of cells from each treatment group were scored for the number of AVs. The data are represented as AVs per 100 μm^2; $n = 20$ images representative of each group. Data represent mean ± SD; *$P < 0.05$. (*B*) WB analysis of LC3B and Cav-1. β-actin served as standard. (*C*) Increased apoptosis in Cav-1-siRNA infected Beas-2B cells by CSE. Cells were transfected with siRNA for 48 h, and followed by CSE treatment at the indicated concentrations for an additional 24 h. Cell lysates were then analyzed for cleaved caspase-3 and cleaved poly(ADP ribose) polymerase. β-Actin served as the standard. (*D*) Cav-1 protects epithelial cells from CSE-induced cell death. Beas-2B cells treated with Cav-1-siRNA were exposed to CSE as indicated for 24 h, and cell viability was measured.

Discussion

Our studies strongly suggest that LC3B exerts an important propathogenic role with respect to CS-induced emphysema development, by up-regulating apoptotic cell death. *LC3B*$^{-/-}$ mice were shown to be relatively resistant to changes in apoptotic indices and airspace induced by chronic CS exposure relative to their WT counterparts. As autophagic proteins play important roles in organ (i.e., mammary gland, nervous system) development (28, 29), we cannot exclude the possibility that the basal airspace enlargement of *LC3B*$^{-/-}$ mice, as detected by MLI, may reflect impaired lung development in these mice. On the contrary, analysis of alveolar diameters did not support a significant basal airspace enlargement of *LC3B*$^{-/-}$ mice. Basal airspace enlargement has been observed in other KO mouse models of critical signaling molecules, including Smad3 (30), TLR4 (31), and TGF-β-R-II (32), suggesting that molecules important in regulating cell proliferation, differentiation, or immune system function, are essential to maintain basal lung structure.

Our in vitro experiments suggest that LC3B plays a regulatory role in extrinsic apoptosis activation, through a dynamic interaction with Fas protein. These results are consistent with our previous observations that siRNA-dependent knockdown of LC3B conferred protection against epithelial cell apoptosis induced by CSE (6). The interaction of LC3B with Fas is facilitated by Cav-1, which acts as a plasma membrane anchor for these proteins. The requirement for Cav-1 in LC3B/Fas interaction, as well as reciprocal complex formation between Cav-1 and LC3B or Fas, suggests the formation of a multiprotein complex that can include all three proteins. Based on our studies, we determined that Cav-1 functions as an anchor for both Fas and LC3B; however, LC3B and Fas bind with Cav-1 at distinct binding sites (Fig. S6). The data further suggest that LC3B knockdown inhibits apoptosis by increasing Cav-1-dependent Fas sequestration. Whether the functional role of LC3B in cell death involves autophagic functions of this protein remains unclear. Previously, we have reported that cells genetically deficient in another major autophagic protein, Beclin 1, were resistant to CS-induced extrinsic apoptosis (33). A recent study suggested that

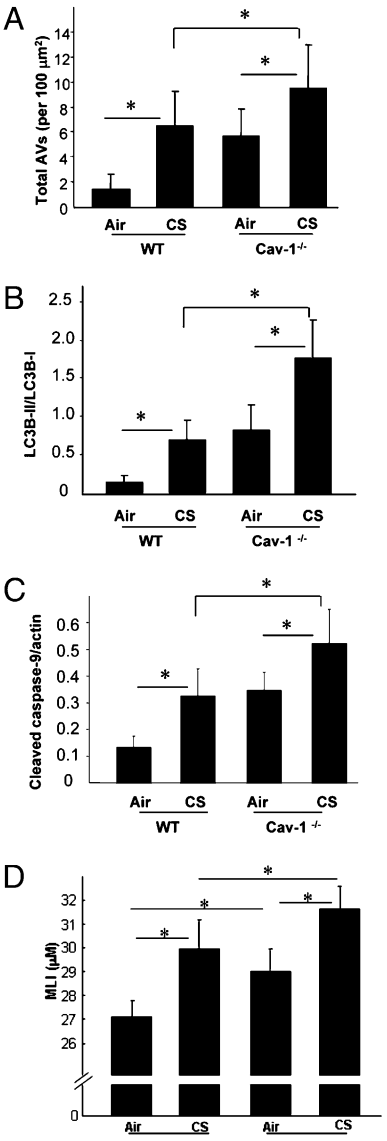

Fig. 5. Cav-1 regulates CS-induced autophagy and apoptosis in vivo. WT C57BL/6 or *Cav-1*$^{-/-}$ mice were exposed to chronic CS exposure for 3 mo (each group, $n = 5$). (*A*) EM images were scored for number of AVs. The data are represented as AVs per 100 μm^2; $n = 20$ images representative of each group. Western blot analysis and corresponding quantification for the LC3B-II/LC3B-I ratio (*B*) and cleaved caspase-9 (*C*) in CS-exposed mouse lungs. (*D*) MLI scoring of mouse lungs exposed to CS. Data represent mean ± SD; $^*P < 0.05$. Representative images of mouse lungs with H&E staining are shown in Fig. S5.

the protective role of resveratrol, a natural antioxidant, in COPD pathogenesis may depend on the inhibition of CS-induced autophagy (34). Further experimentation to determine the role of autophagic flux in these phenotypic observations may be warranted.

Mutation of the Cav-1-binding site in LC3B (Y113A) resulted in loss of LC3B/Cav1 interaction in vitro. Transfection of LC3B Y113A resulted in reduced apoptosis in response to CS relative to WT LC3B. These results indicate that the interaction of LC3B with Cav-1 is required for the proapoptotic function of LC3B in this model. The reduced effectiveness of LC3B Y113A relative to WT LC3B at promoting apoptosis (Fig. 3*C*), may be a result of the apparent increase in Cav-1-Fas interaction (Fig. 3*B*) and consequent reduced activation of the extrinsic apoptotic pathway. The dissociation of LC3B and Fas from Cav-1 is stimulated by CSE, which permits further progression of the extrinsic apoptotic pathway. The elucidation of the molecular mechanism(s) for the dissociation of these regulatory complexes by prodeath stimuli requires further investigation.

Our studies also suggest that Cav-1 can exert a functional role in CS-induced emphysema development by downregulating autophagic and apoptotic pathways. The recent studies of Volonte et al. report an emphysema-resistant phenotype in *cav-1*$^{-/-}$ mice (35). The authors proposed a role for Cav-1 in CS-induced emphysema based on the promotion of epithelial cell senescence, although autophagy and apoptosis were not examined (35). In our current study, we show that *cav-1*$^{-/-}$ mice are more susceptible to CS-induced lung injury, with respect to activation of lung cell apoptosis and AV accumulation in lung tissue. In agreement with our current findings, a recent study has also demonstrated increased autophagy in several organs in the *Cav-1*$^{-/-}$ mice (36).

Although the *Cav-1*$^{-/-}$ mice had a basal lung airspace enlargement, they were also more susceptible to the CS-induced lung injury and displayed a further enlarged airspace. The apparent phenotypic differences between our studies and those of Volonte et al. (35) remain unclear at this point; however, we have replicated our experiments with two independent models of inhalation CS, a nose-only inhalation delivery system used in Figs. 1 and 5, and a secondhand smoke inhalation using a total-body box. Similar results with respect to autophagic and apoptotic phenotypes in *Cav-1*$^{-/-}$ mice were observed with both smoke exposure systems (Fig. 5*D* and Figs. S5 and S7). Our results of airspace enlargement in *cav-1*$^{-/-}$ mice are further supported by observations of increased apoptosis in *cav-1*$^{-/-}$ lungs.

In summary, we demonstrate that dynamic interactions of the autophagic protein LC3B with Cav-1 and Fas regulate CS-induced lung epithelial cell apoptosis. Our study provides a mechanism by which LC3B cross-regulates apoptosis, and also suggests a pivotal role for LC3B in emphysema development, which may lead to new therapeutic targets for COPD.

Methods

Mice. *LC3B*$^{-/-}$ mice were provided by Marlene Rabinovitch (Stanford University, Stanford, CA), as described elsewhere (37). WT C57BL/6 mice and *Cav-1*$^{-/-}$ mice were from Jackson Laboratories. All animal experiment protocols were approved by the Harvard Standing Committee for Animal Welfare or the University of Pittsburgh Institutional Animal Care and Use Committee.

In Vivo CS Exposure. Mice were exposed to CS from four unfiltered cigarettes 5 d/wk for 3 mo using a nose-only smoking apparatus with the chamber adapted for mice, as previously described (38).

Lung Morphometry. Lung samples were processed for morphometric analysis, and airspace enlargement was quantified by using a previously published, automated image processing algorithm (16), and also using the MLI method (39–41) as described in detail in *SI Methods*.

Cell Culture, CSE Treatment, and Cell Viability Assay. Human lung epithelial Beas-2B cells were maintained in DMEM containing 10% FBS and antibiotics. Primary mouse lung fibroblasts were cultured as described (24) and used for experiments as subconfluent monolayers at passages seven to 12. Aqueous CSE was prepared as previously described (6). Additional details are provided in *SI Methods*. Cell viability was determined by the 3-(4,5-dimethylthiazol-2-yl)-2,5-diphenyl tetrazolium bromide assay as described previously (6).

Transmission EM. Lung tissue sections were processed for EM and analyzed for autophagic vacuole formation as previously described (6). See *SI Methods* for additional details.

Immunofluorescence Staining. After treatment, Beas-2B cells were fixed with 4% paraformaldehyde and analyzed with the immunofluorescence staining protocol as described previously (24). Samples were viewed with an Olympus

Fluoview 300 confocal laser scanning head with an Olympus IX70 inverted microscope.

DNA Constructs. Human WT LC3B cDNA (pCMV6-XL5-LC3B) was obtained from Origene, and mutagenesis was performed using the QuikChange II Site-Directed Mutagenesis Kit (Stratagene). The Cav-1 WT (WT-Cav-1) expression clone and the Cav-1 CSD (residues 82–101)-deleted mutant (ΔCSD) were gifts from C. Tiruppathi (University of Illinois at Chicago, Chicago, IL). The Fas wt and Fas C199S expression clones were kind gifts from M. E. Peter (University of Chicago, Chicago, IL).

siRNA and cDNA Transfection. Human LC3B-siRNA and Cav-1-siRNA were from Santa Cruz Biotechnology. The siRNA was transfected into cells by using the transfection reagent (Santa Cruz Biotechnology). Human WT LC3B cDNA and its mutant derivatives were transfected into Beas-2B cells by using Lipofectamine 2000 (Invitrogen).

Immunoprecipitation and Western Blot Analysis. Immunoprecipitation and immunoblotting were performed essentially as previously described (6, 20, 24). *SI Methods* provides additional details.

Statistical Analysis. Results were expressed as means ± SD from at least three independent experiments. Differences in measured variables between experimental and control group were assessed by using the Student *t* test. Statistically significant difference was accepted at $P < 0.05$.

ACKNOWLEDGMENTS. We thank Dr. Beth Levine (University of Texas, Austin, TX) for the *BECN*$^{+/-}$ mice, Marlene Rabinovitch (Stanford University, Stanford, CA) for the *LC3B*$^{-/-}$ mice, and Meng Zhang for expert technical assistance. We are also grateful to Dr. Bela Suki (Boston University) for assistance with emphysema analysis. This work was supported by National Institutes of Health Grants R01-HL60234, R01-HL55330, and R01-HL079904 (to A.M.K.C.), and R01-HL090757 (to H.P.).

1. Lopez AD, Murray CC (1998) The global burden of disease, 1990-2020. *Nat Med* 4: 1241–1243.
2. Rabe KF, et al.; Global Initiative for Chronic Obstructive Lung Disease (2007) Global strategy for the diagnosis, management, and prevention of chronic obstructive pulmonary disease: GOLD executive summary. *Am J Respir Crit Care Med* 176: 532–555.
3. Yoshida T, Tuder RM (2007) Pathobiology of cigarette smoke-induced chronic obstructive pulmonary disease. *Physiol Rev* 87:1047–1082.
4. Petrache I, et al. (2005) Ceramide upregulation causes pulmonary cell apoptosis and emphysema-like disease in mice. *Nat Med* 11:491–498.
5. Kasahara Y, et al. (2000) Inhibition of VEGF receptors causes lung cell apoptosis and emphysema. *J Clin Invest* 106:1311–1319.
6. Chen ZH, et al. (2008) Egr-1 regulates autophagy in cigarette smoke-induced chronic obstructive pulmonary disease. *PLoS ONE* 3:e3316.
7. Ryter SW, Chen ZH, Kim HP, Choi AM (2009) Autophagy in chronic obstructive pulmonary disease: Homeostatic or pathogenic mechanism? *Autophagy* 5:235–237.
8. Levine B, Klionsky DJ (2004) Development by self-digestion: Molecular mechanisms and biological functions of autophagy. *Dev Cell* 6:463–477.
9. Xie Z, Klionsky DJ (2007) Autophagosome formation: Core machinery and adaptations. *Nat Cell Biol* 9:1102–1109.
10. He C, Klionsky DJ (2009) Regulation mechanisms and signaling pathways of autophagy. *Annu Rev Genet* 43:67–93.
11. Kabeya Y, et al. (2000) LC3, a mammalian homologue of yeast Apg8p, is localized in autophagosome membranes after processing. *EMBO J* 19:5720–5728.
12. Berry DL, Baehrecke EH (2008) Autophagy functions in programmed cell death. *Autophagy* 4:359–360.
13. Shimizu S, et al. (2004) Role of Bcl-2 family proteins in a non-apoptotic programmed cell death dependent on autophagy genes. *Nat Cell Biol* 6:1221–1228.
14. Suzuki M, et al. (2009) Curcumin attenuates elastase- and cigarette smoke-induced pulmonary emphysema in mice. *Am J Physiol Lung Cell Mol Physiol* 296:L614–L623.
15. Bartalesi B, et al. (2005) Different lung responses to cigarette smoke in two strains of mice sensitive to oxidants. *Eur Respir J* 25:15–22.
16. Parameswaran H, Majumdar A, Ito S, Alencar AM, Suki B (2006) Quantitative characterization of airspace enlargement in emphysema. *J Appl Physiol* 100:186–193.
17. Barnhart BC, Lee JC, Alappat EC, Peter ME (2003) The death effector domain protein family. *Oncogene* 22:8634–8644.
18. Green DR (2005) Apoptotic pathways: Ten minutes to dead. *Cell* 121:671–674.
19. Gajate C, et al. (2004) Intracellular triggering of Fas aggregation and recruitment of apoptotic molecules into Fas-enriched rafts in selective tumor cell apoptosis. *J Exp Med* 200:353–365.
20. Park JW, et al. (2008) Protein kinase C α and ζ differentially regulate death-inducing signaling complex formation in cigarette smoke extract-induced apoptosis. *J Immunol* 180:4668–4678.
21. Schlegel A, Lisanti MP (2001) The caveolin triad: Caveolae biogenesis, cholesterol trafficking, and signal transduction. *Cytokine Growth Factor Rev* 12:41–51.
22. Couet J, Li S, Okamoto T, Ikezu T, Lisanti MP (1997) Identification of peptide and protein ligands for the caveolin-scaffolding domain. Implications for the interaction of caveolin with caveolae-associated proteins. *J Biol Chem* 272:6525–6533.
23. Zhao YY, et al. (2002) Defects in caveolin-1 cause dilated cardiomyopathy and pulmonary hypertension in knockout mice. *Proc Natl Acad Sci USA* 99:11375–11380.
24. Wang XM, et al. (2006) Caveolin-1: A critical regulator of lung fibrosis in idiopathic pulmonary fibrosis. *J Exp Med* 203:2895–2906.
25. Hoetzel A, et al. (2009) Carbon monoxide prevents ventilator-induced lung injury via caveolin-1. *Crit Care Med* 37:1708–1715.
26. Jin Y, et al. (2008) Deletion of caveolin-1 protects against oxidative lung injury via up-regulation of heme oxygenase-1. *Am J Respir Cell Mol Biol* 39:171–179.
27. Jin Y, et al. (2009) Caveolin-1 regulates the secretion and cytoprotection of Cyr61 in hyperoxic cell death. *FASEB J* 23:341–350.
28. Gajewska M, Sobolewska A, Kozlowski M, Motyl T (2008) Role of autophagy in mammary gland development. *J Physiol Pharmacol* 59(Suppl 9):237–249.
29. Winslow AR, Rubinsztein DC (2008) Autophagy in neurodegeneration and development. *Biochim Biophys Acta* 1782:723–729.
30. Chen H, et al. (2005) Abnormal mouse lung alveolarization caused by Smad3 deficiency is a developmental antecedent of centrilobular emphysema. *Am J Physiol Lung Cell Mol Physiol* 288:L683–L691.
31. Zhang X, Shan P, Jiang G, Cohn L, Lee PJ (2006) Toll-like receptor 4 deficiency causes pulmonary emphysema. *J Clin Invest* 116:3050–3059.
32. Chen H, et al. (2008) TGF-beta receptor II in epithelia versus mesenchyme plays distinct roles in the developing lung. *Eur Respir J* 32:285–295.
33. Kim HP, et al. (2008) Autophagic proteins regulate cigarette smoke-induced apoptosis: Protective role of heme oxygenase-1. *Autophagy* 4:887–895.
34. Hwang JW, et al. (2010) Cigarette smoke-induced autophagy is regulated by SIRT1-PARP-1-dependent mechanism: Implication in pathogenesis of COPD. *Arch Biochem Biophys* 500:203–209.
35. Volonte D, Kahkonen B, Shapiro S, Di Y, Galbiati F (2009) Caveolin-1 expression is required for the development of pulmonary emphysema through activation of the ATM-p53-p21 pathway. *J Biol Chem* 284:5462–5466.
36. Le Lay S, et al. (2010) The lipoatrophic caveolin-1 deficient mouse model reveals autophagy in mature adipocytes. *Autophagy* 6:754–763.
37. Cann GM, et al. (2008) Developmental expression of LC3alpha and beta: Absence of fibronectin or autophagy phenotype in LC3beta knockout mice. *Dev Dyn* 237: 187–195.
38. Hautamaki RD, Kobayashi DK, Senior RM, Shapiro SD (1997) Requirement for macrophage elastase for cigarette smoke-induced emphysema in mice. *Science* 277: 2002–2004.
39. Dunhill MS (1962) Quantitative methods in the study of pulmonary pathology. *Thorax* 17:320–328.
40. Weibel ER (1979) *Stereological Methods* (Academic Press, London).
41. Tomkeieff SI (1945) Linear intercepts, areas and volumes. *Nature* 155:24.